Supporting Online Material

Materials and Methods

Protein expression and purification. DNA encoding residues 160–217 of human CEP55 (EABR) was amplified using the polymerase chain reaction (PCR). The products were subcloned into the parallel GST2 vector (S*1*). CEP55-EABR was fused to an N-terminal GST tag followed by a tobacco etch virus (TEV) protease cleavage site. Peptides containing residues 797–809 and 791–809 of human ALIX designed with an extra one or two N-terminal and C-terminal Asp residues to improve solubility. DQAQGPPYPTYPGYD (crystallization) and DDGSAPPPQAQGPPYPTYPGYDD (solution experiments) were obtained from New England Peptide. Site-directed mutants were generated using the Quik-Change mutagenesis kit (Stratagene). All constructs were verified by DNA sequencing. CEP55-EABR was expressed in *Escherichia coli* BL21 CodonPlus(DE3)-RIL (Stratagene) at 37 °C for 5 h by induction with 0.5 mM isopropylthiogalactoside (IPTG) when cells reached an A_{600} of 0.8. Cells were lysed by sonication in phosphate buffered saline (PBS) and centrifuged. The supernatant was applied to a glutathione-Sepharose column (GE Healthcare). The fusion protein was cleaved with His_6-tagged TEV protease while bound to the matrix at 4 °C overnight. CEP55-EABR was further purified by gel filtration (Superdex 200 16/60) and ion exchange (5 ml HiTrap Q HP) chromatography (GE Healthcare). Fractions were pooled, concentrated to 7 mg ml^{-1} in 20 mM Tris (pH 7.5) and 100 mM NaCl (buffer A). Selenomethionyl protein was purified in the same way as the native protein. All the mutants were purified as described above.

Isothermal titration calorimetry. CEP55-EABR (0.2 mM, placed in the sample cell), ALIX peptide (DDGSAPPPQAQGPPYPTYPGYDD, 1.6 mM, injectant), and TSG101 peptide (DDASYPPYQATGPPNTSYMPGDD, 1.4 mM, injectant) were dissolved in 20 mM Tris-HCl (pH 7.5) and 100 mM NaCl. Titrations (35 injections of 5 µl ALIX or TSG101 peptides each) were performed at 27 °C using a VP-ITC Microcalorimeter (MicroCal), and data were analyzed using Origin software (Origin Lab).

Competition assay. 70 μg of CEP55-EABR was incubated with 350 μg of GST–$ALIX_{795\_811}$ for 1 h at 4 °C. For competition, TSG101 peptides (20, 40, 160, and 250 μg, respectively) were added. The mixtures were then absorbed with glutathione-Sepharose beads (GE Healthcare) for 1 h, and the beads were washed extensively by 20 mM Tris (pH 7.5) and 100 mM NaCl. Bound proteins were eluted, separated by SDS/PAGE, and stained with Coomassie Blue.

Analytical ultracentrifugation. Sedimentation velocity experiments were conducted in duplicate at 4.0°C on a Beckman Coulter XL-A or XL-I analytical ultracentrifuge. Samples of CEP55-EABR, ALIX and TSG101 in 20 mM Tris pH 7.5, 100 mM NaCl (loading volume of 400 μL) were studied at various loading concentrations and ratios at 60 krpm. 300 scans were acquired as single absorbance measurements (λ=280 nm) at 5 minute intervals using a radial spacing of 0.003 cm and analyzed in SEDFIT 11.3 (S*2*) to obtain a sedimentation coefficient, *s* or a c(*s*) distribution. Values were corrected to $s_{20,w}$ or c($s_{20,w}$) using solvent parameters calculated in SEDNTERP 1.09 (http://www.jphilo.mailway.com/). c(*s*) analyses were carried out using an $s_{20,w}$ range of 0.03 to 6.5 with a linear resolution of 100 and a confidence level (F-ratio) of 0.68. Excellent data fits were obtained with rmsd values of 0.0036 to 0.0082 absorbance units. Sedimentation equilibrium experiments were conducted at 4.0°C and data were acquired as an average of 8 absorbance measurements (λ=280 and 250 nm, loading volume of 130 μL) at a radial spacing of 0.001 cm. ALIX, TSG101 and their 1:1 mixture at a loading concentration of 150 μM were analyzed at 50, 55 and 60 krpm. CEP55-EABR, at a loading concentration of 62.5 μM, and mixtures with ALIX and/or TSG101 were studied at rotor speeds of 25 to 45 krpm. Data were analyzed globally in terms of various non-interacting solute models using SEDPHAT 4.3 (S*3*) with or without mass conservation constraints.

Crystallization and data collection. Before crystallization, equal volumes of CEP55-EABR (7 mg ml^{-1}) in buffer A and ALIX peptide (8.7 mg ml^{-1}) in 20 mM Tris pH 8.0 was mixed and incubated at 4 °C for an hour. Crystals of the CEP55-EABR–$ALIX_{797\_809}$

complex were grown at 21 °C using hanging-drop vapor diffusion by mixing 2 µl of the protein complex solution with 2 µl of 100 mM MES buffer (pH 6.0) and 22% PEG 6000. Crystals were cryo-protected by soaking to 100% Paratone-N solution and flash frozen in liquid nitrogen. Selenium MAD and native experimental data were collected at 95^{o} K at APS SER-CAT Beamline 22-ID, and processed using HKL2000 (HKL Research).

Structure determination and refinement. Two of two expected selenium sites were located and refined using SOLVE (S*4*), and initial phases were calculated at 3.0 Å. An interpretable electron density map was obtained after density modification and phase extension to 2.2 Å with RESOLVE (S*5*). The model was built manually in COOT (S*6*). Subsequent rounds of model adjustment, simulated annealing and thermal factor refinement were performed with CNS (S*7*). During the final refinement stages, water molecules were inserted into the protein model. Statistics are summarized in Supplementary Table 1. The asymmetric unit contains a homodimer of the CEP55 and one ALIX peptide, where chains A and B correspond to CEP55-EABR and chain C corresponds to the ALIX peptide. This model includes 113 water molecules. 100 % of the residues are in the most allowed region of the Ramachandran plot. No electron density was observed for residues 160–164 and 211–217 in chain A, and 160–166 and 209–217 in chain B of CEP55-EABR.

Surface plasmon resonance. The binding of wild-type and mutants of CEP55-EABR and ALIX proteins was measured with a Biacore T100 system at 25 °C with a flow rate of 10 µl min^{-1}. GST–ALIX$_{795–811}$ (wild-type, G800A, P801A, P802A, and Y806A mutants) and GST–CEP55-EABR (W184A, Y187A, R191A, and E192A mutants) were immobilized on a CM5 surface via covalent linkage to the N terminus of GST. A CM5 chip was activated using 1:1 N-hydroxysuccinimide (NHS)/1-ethyl-3-(3-dimethylaminopropyl)carbodiimide (EDC) at a flow rate of 5 µl min^{-1} for 7 min. Each protein sample (each 10 µM) in 10 mM acetate buffer (pH 4.5) was passed over separate flow cells at 5 µl min^{-1} for 7 min, and this was followed by a blocking step using ethanolamine (1 M, pH 8.5) at 5 µl min^{-1} for 7 min. All binding experiments were performed in 20 mM Tris (pH 7.5) and 100 mM NaCl. Binding of mutant CEP55-EABR

proteins except D188A to ALIX wild-type was measured by passing the $ALIX_{791–809}$ peptide (DDGSAPPPQAQGPPYPTYPGYDD) over flow cells coupled to GST–CEP55-EABR mutants (W184A, Y187A, R191A, and E192A respectively) with association and dissociation times of 20 s and 20 s, respectively. Binding of mutant ALIX proteins to CEP55-EABR wild-type was measured by passing CEP55-EABR over flow cells coupled to GST–$ALIX_{795–811}$ mutants (G800A, P801A, P802A, and Y806A, respectively) with association and dissociation times of 300 s and 400 s, respectively. Between subsequent injections of all the proteins, surfaces were regenerated with an injection of 20 mM Tris (pH 7.5) and 500 mM NaCl for 10–30 s at 10 μl min^{-1}.

Constructs for cell biology. Human CEP55 in pEGFP-C3 vector and TSG101 in pEGFP-C2 vector, both containing N-terminal GFP, were kindly provided by Kerstin Kutsche (Universitätsklinikum Hamburg-Eppendorf, Germany) and Eric O. Freed (NCI, Frederick, MD), respectively. GFP-ALIX construct was cloned into the EcoRI/BamHI sites of Clontech (Mountain View, CA) pEGFP-C2 vector. Site-directed mutants of GFP-CEP55, GFP-ALIX, and GFP-TSG101 were generated using the Quik-Change mutagenesis kit (Stratagene), and were verified by DNA sequencing. Both mCherry-ALIX and mCherry-TSG101 constructs were cloned into Clontech pmCherry-C2.

Cell culture and fluorescent imaging

HeLa cells were transfected at low confluency (20-30%) with the designated plasmids and fixed or imaged live 48 h post-transfection using a confocal microscope. Fixation was performed with 4% Paraformaldehyde. Monoclonal α-tubulin antibodies (DM1A Sigma Aldrich) were used for microtubule staining.

Imaging conditions and data analysis. Fixed or live cells were imaged with a confocal microscope (LSM 510, Zeiss or Fluoview FV1000, Olympus) with a 60X or 63X NA 1.4 oil objectives. Brightness and contrast were adjusted in Photoshop 7.0 (Adobe).

Modeling. The crystal structure of the EABR fragment of CEP55 suggested to us a model for the N-terminal half of the CEP55 dimer. Nearly all of the CEP55 sequence is

predicted to form a coiled coil (S*8-10*) based on sequence analysis (S*11*). Most of these sequence analyses have predicted a gap in the coiled coil corresponding to the EABR region (S*8,S9, S12*), and this region has been postulated to serve as a hinge connecting other coiled regions, in addition to its ALIX and ESCRT binding function (S*12*). We found that the entire EABR region is a coiled coil. The coil maintains register across the unusual central two heptad repeats. Moreover, although there is a ~20 residue gap between the C-terminus of the EABR and the start of the strongly predicted C-terminal coiled-coil, the crystallized EABR overlaps with the predicted coiled coil on the N-terminal side. A model of residues 1–163 of CEP55 coiled coil structure was constructed using the crystal structure of human beta-myosin S2 (PDB code 2FXO) (S*13*) as a template. The model was built manually, extending a repeating unit of coiled coil in a linear fashion. The repeating units were overlapped in order to maintain the pitch of the coiled coil, and assigned with the correct amino acid residues of CEP55. The overlapping helices were then removed from the model. The ESCRT-I core (PDB code 2P22) (S*14*) and UEV domain (PDB code 1M4Q) (S*15*), and ALIX (PDB code 2OEV) (S*16*) were docked onto the separate molecules of CEP55 as suggested by AUC and competition experiments. The CHMP4 C-terminal helix was obtained from PDB code (3C3O) and modeled by superimposing its Bro1 domain complex on the full-length ALIX structure (PDB code 2OEV).

Supplementary Figure Legends

Figure S1. Minimal interacting fragments of CEP55 and ALIX.
CEP55 constructs shown in blue were insoluble when expressed in E. coli, and those shown in red were soluble. All CEP55 and ALIX constructs were made by GST-fusion at N-terminus.

Figure S2. Analytical ultracentrifugation of CEP55-EABR:peptide mixtures.
The top panel shows curves for the components in isolation for 50 μM (brown trace) and 100 μM (green trace) CEP55, 170 -190 μM peptide; the second and third panels show mixtures of CEP55-EABR with TSG101 and ALIX, respectively, at various stoichiometries; and the bottom panel mixtures of CEP55-EABR with combinations of both peptides. The CEP55-EABR concentration is 56 μM.

Figure S3. CEP55-EABR is a monodisperse dimer.
(A) Sedimentation velocity profiles at 60 krpm, 280 nm and 4.0°C obtained for 50 μM CEP55 –EABR. Scans at 20 minute intervals are shown with only every third experimental data point. The solid lines are best fit curves to a single species corresponding to a dimeric CEP55-EABR; the pooled residuals corresponding to this fit are shown in the middle panel. Residuals for all of the 160 scans used in the analysis are shown in bitmap format in the top panel. **(B)** Sedimentation equilibrium absorbance profiles at 250 (left panel) and 280 nm (right panel) versus the radius r, for 62.5 μM CEP55-EABR. Data were collected at 25 (orange), 30 (yellow), 35 (green), 40 (cyan) and 45 (brown) krpm and analyzed globally in terms of a single ideal solute. The best fits obtained, shown as black lines through the experimental points, demonstrate that the CEP55-EABR is a monodisperse dimer. The residuals corresponding to this best fit are shown above each plot.

Figure S4. The CEP55-EABR dimer binds one equivalent of ALIX.

(A) Sedimentation velocity profiles at 60 krpm, 280 nm and 4.0°C obtained for a 2:1 stoichiometric mixture of CEP55 –EABR (56 μM) and ALIX. Scans at 25 minute intervals are shown with only every third experimental data. The solid lines are best fit curves to a continuous c(s) analysis (see Fig. 1E) showing the presence of a 2:1 complex and slight excess of ALIX; the pooled residuals corresponding to this fit are shown in the middle panel. Residuals for all of the 200 scans used in the analysis are shown in bitmap format in the top panel. **(B)** Sedimentation equilibrium absorbance profiles at 250 (left panel) and 280 nm (right panel) versus the radius r, for a mixture of 62.5 μM CEP55-EABR and 66.5 μM ALIX. Data were collected at 25 (orange), 30 (yellow), 35 (green), 40 (cyan) and 45 (brown) krpm and analyzed globally in terms of two non-interacting solutes. The best fits obtained, shown as black lines through the experimental points, demonstrate that the presence of a 2:1 CEP55-EABR:ALIX complex, and free peptide. The residuals corresponding to this best fit are shown above each plot. Mass conservation constraints on the sedimentation equilibrium data return, within the error of the method, complex and peptide concentrations identical to those expected for a 2:1 complex stoichiometry.

Figure S5. Experimental electron density.
Density-modified MAD synthesis after phase extension to 2.2 Å, contoured at 1.0 σ.

Figure S6. Abnormal separation of the two strands of the CEP55 coiled coil.

Figure S7: Midbody localization of wild-type and mutant GFP-CEP55 . HeLa cells expressing wild-type or mutant GFP-CEP55 (shown in green) were fixed and stained with α–tubulin antibodies (shown in red). The merged image of GFP-CEP55 and α–tubulin is shown. Scale bar = 10 μm

Figure S8: Impaired midbody localization of mCh-TSG101 in mutant GFP-CEP55 expressing cells. HeLa cells were cotransfected with wild-type or mutant GFP-CEP55

and wild-type mCh-TSG101. Cells were imaged live and GFP-CEP55 localization was used as a midbody marker (see Fig. S5 for midbody localization of CEP55 mutants). Cell boundaries are illustrated in the merged image to highlight the midbody region. mCh-TSG101 midbody localization is reduced in cells expressing GFP-CEP55^{R191A} and is hardly detectible in cells expressing GFP-CEP55^{W184A} or GFP-CEP55^{Y187A} mutants.

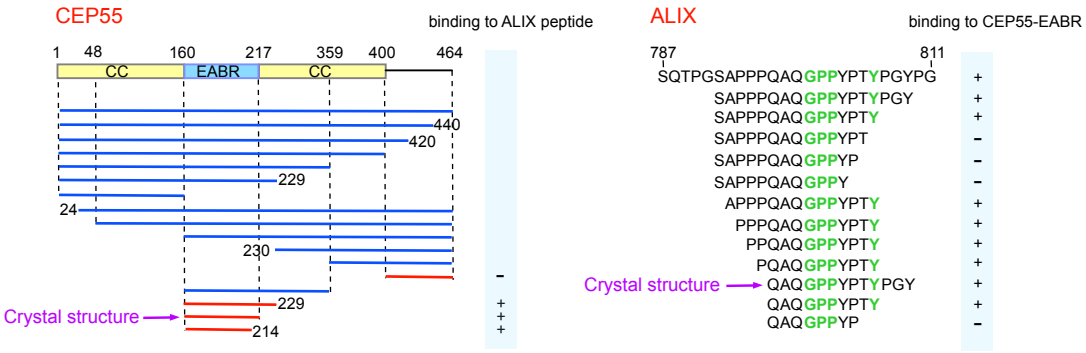
CEP55
binding to ALIX peptide
1
48
160
217
359
400
464
CC
EABR
CC
440
420
229
24
230
229
214
Crystal structure
-
+
+
+
ALIX
binding to CEP55-EABR
787
811
SQTPGSAPPPQAQGPPYPTYPGYPG +
SAPPPQAQGPPYPTYPGY +
SAPPPQAQGPPYPTY +
SAPPPQAQGPPYPT -
SAPPPQAQGPPYP -
SAPPPQAQGPPY -
APPPQAQGPPYPTY +
PPPQAQGPPYPTY +
PPQAQGPPYPTY +
PQAQGPPYPTY +
Crystal structure
QAQGPPYPTYPGY +
QAQGPPYPTY +
QAQGPPYP -

Figure S1

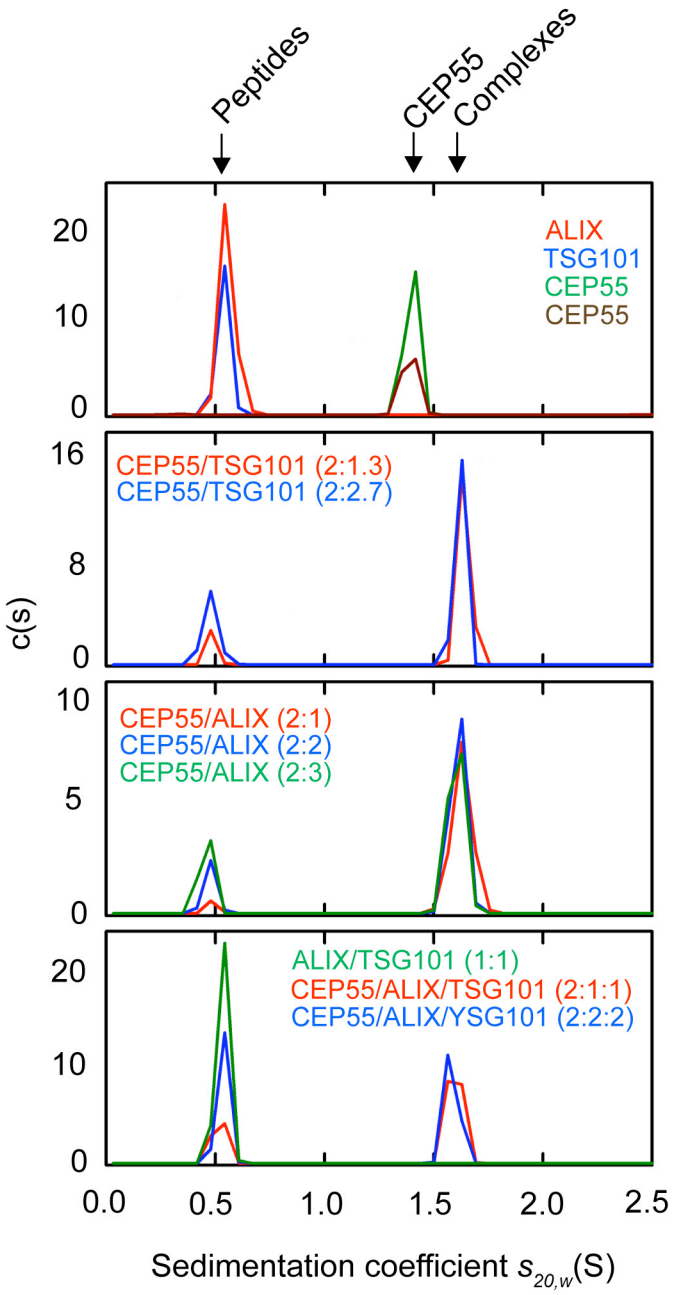
Peptides
CEP55
Complexes
ALIX
TSG101
CEP55
CEP55
CEP55/TSG101 (2:1.3)
CEP55/TSG101 (2:2.7)
CEP55/ALIX (2:1)
CEP55/ALIX (2:2)
CEP55/ALIX (2:3)
ALIX/TSG101 (1:1)
CEP55/ALIX/TSG101 (2:1:1)
CEP55/ALIX/YSG101 (2:2:2)
c(s)
Sedimentation coefficient $s_{20,w}$(S)

Figure S2

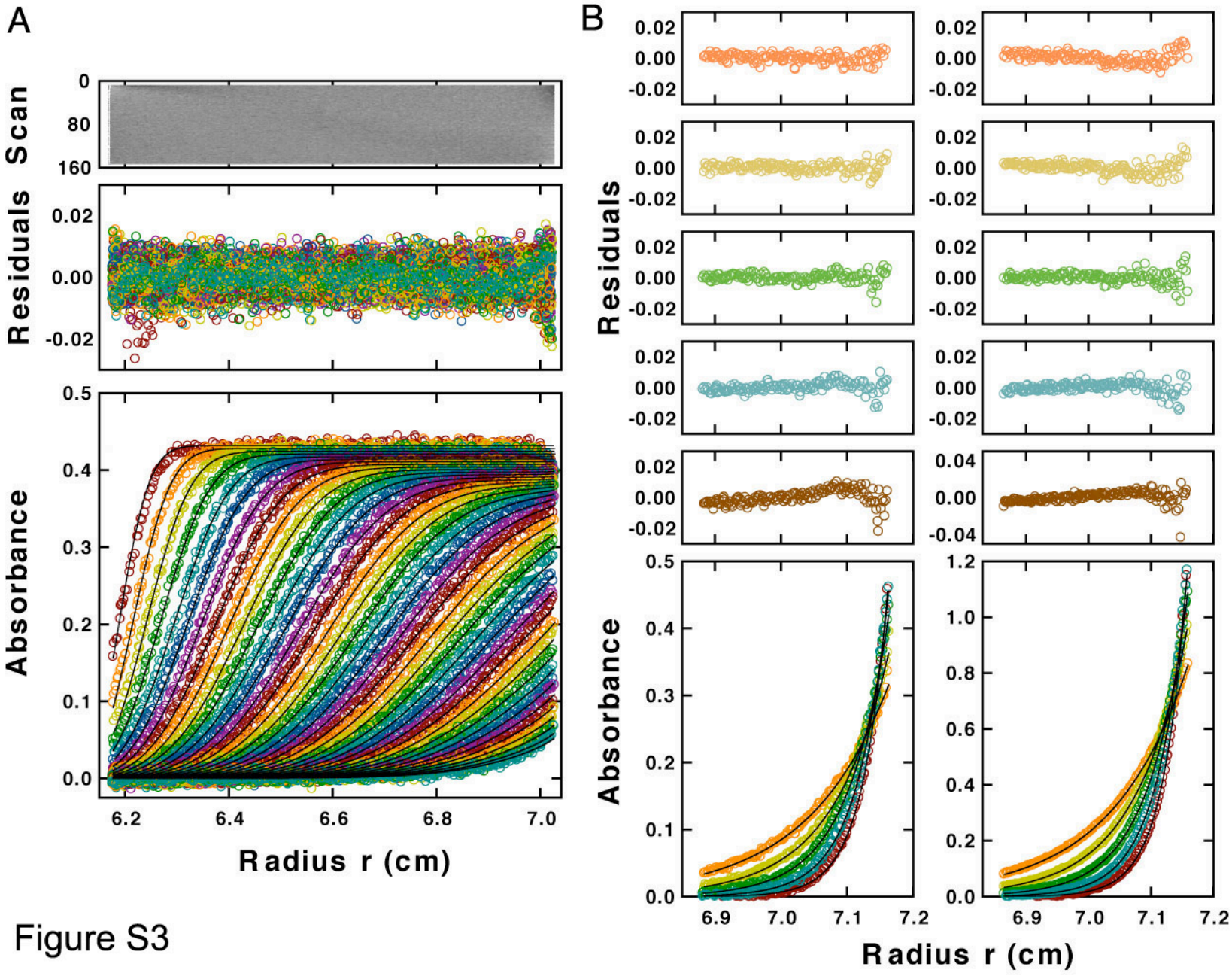
A
Scan
0
80
160
Residuals
0.02
0.00
-0.02
Absorbance
0.5
0.4
0.3
0.2
0.1
0.0
6.2
6.4
6.6
6.8
7.0
Radius r (cm)
B
Residuals
0.02
0.00
-0.02
0.04
-0.04
Absorbance
1.2
1.0
0.8
0.6
0.4
0.2
6.9
7.0
7.1
7.2
Radius r (cm)

Figure S3

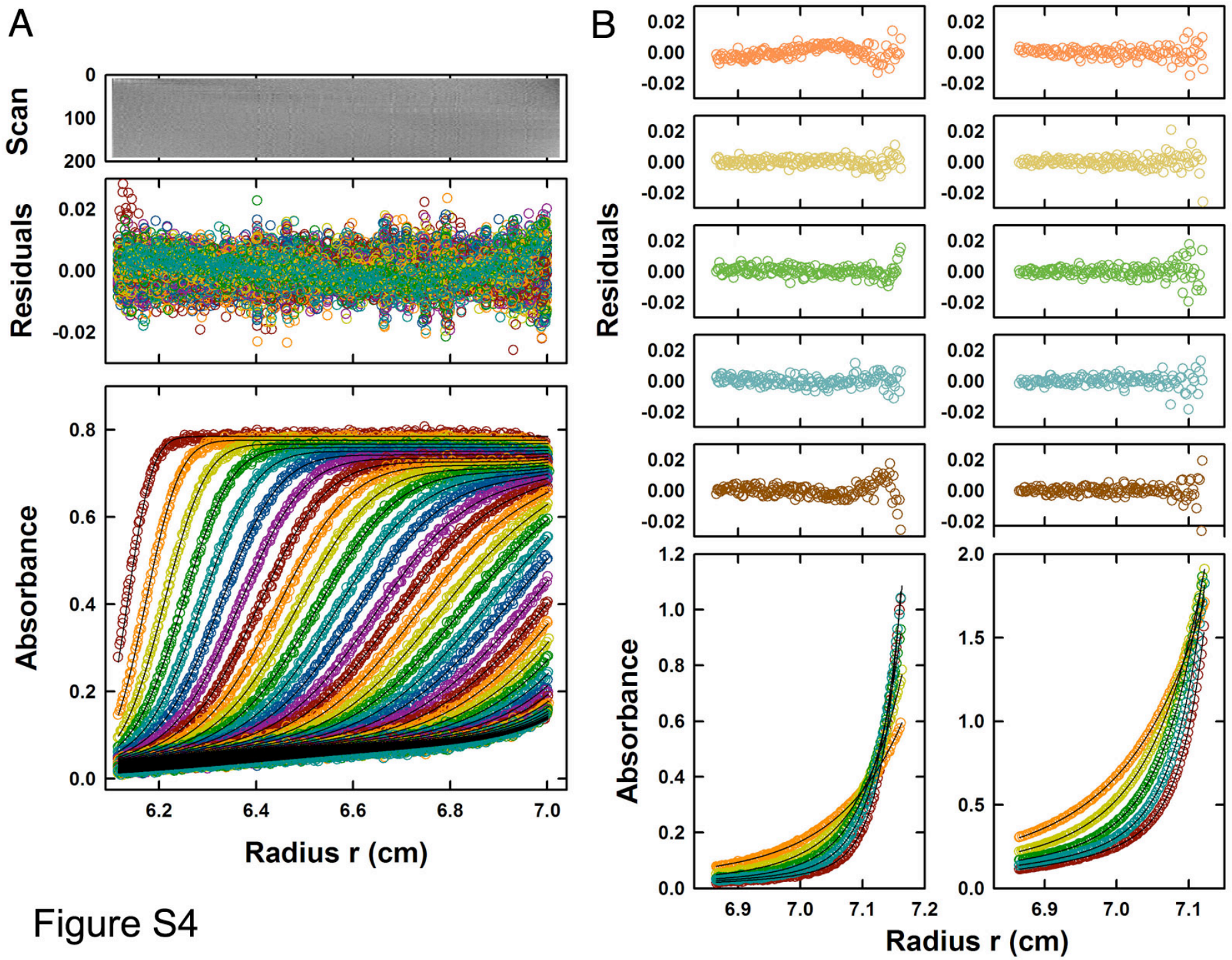
A
Scan
0
100
200
Residuals
0.02
0.00
-0.02
Absorbance
0.8
0.6
0.4
0.2
0.0
6.2
6.4
6.6
6.8
7.0
Radius r (cm)
B
Residuals
0.02
0.00
-0.02
Absorbance
1.2
1.0
0.8
0.6
0.4
0.2
0.0
2.0
1.5
1.0
0.5
0.0
6.9
7.0
7.1
7.2
Radius r (cm)

Figure S4

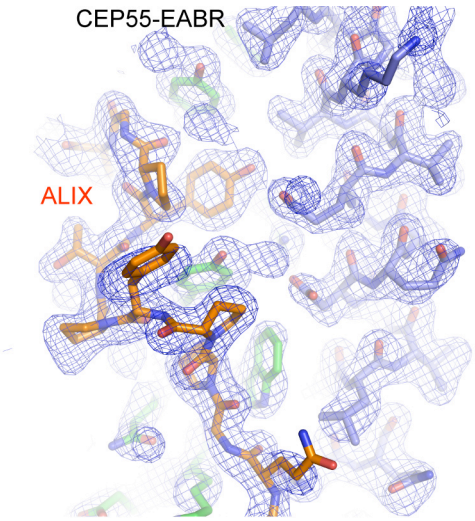

Figure S5

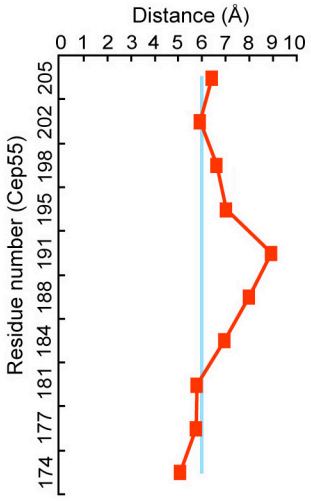
Distance (Å)
0 1 2 3 4 5 6 7 8 9 10
Residue number (Cep55)
174 177 181 184 188 191 195 198 202 205

Figure S6

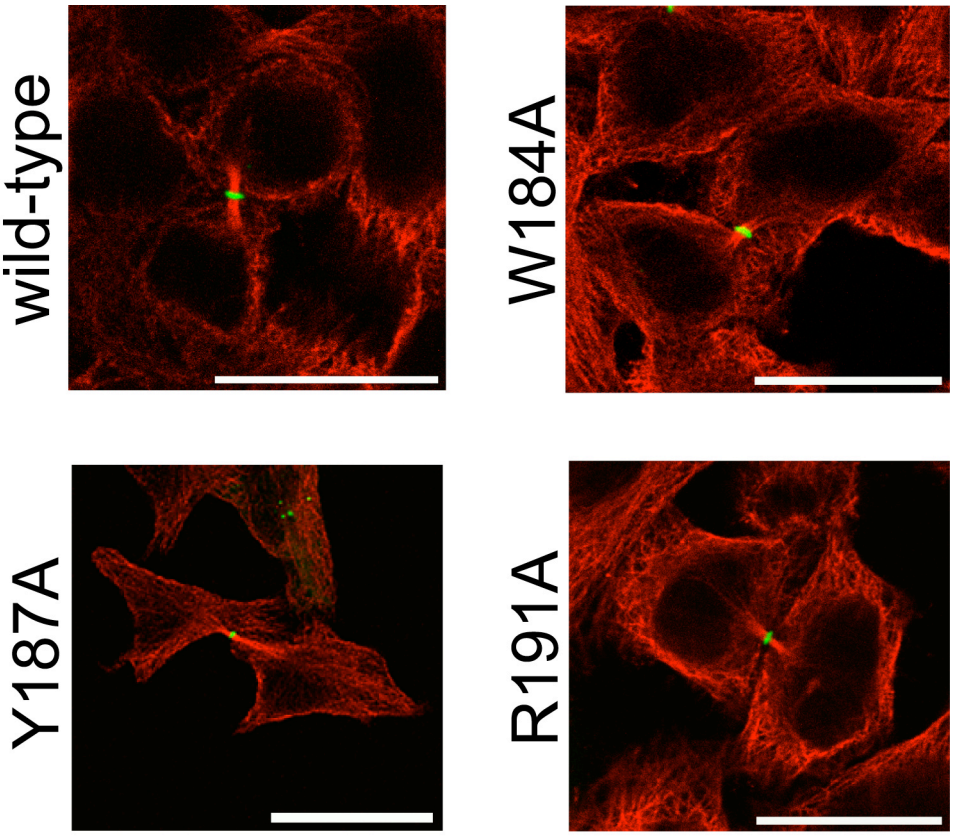

Figure S7

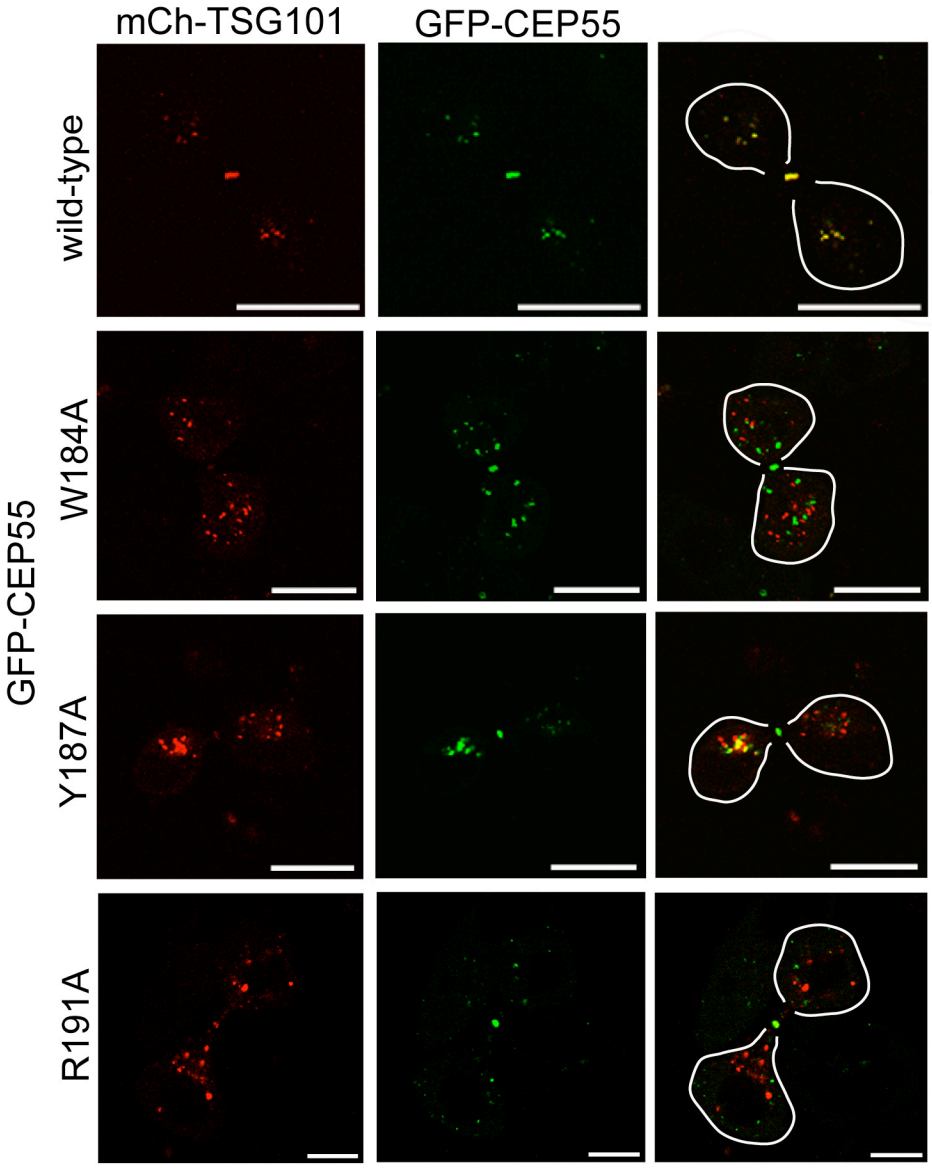

Figure S8

Table S1: Data collection, MAD phasing and refinement statistics

	Native	SeMet		
Data collection				
Space group	$C222_1$	$C222_1$		
Cell dimensions				
a, b, c (Å)	54.6 61.2 88.5	54.3 60.8 91.7		
		Peak	Inflection	Remote
Wavelength (Å)	0.97929	0.97908	0.97935	0.97173
Resolution (Å)	50–2.0 (2.07–2.0)	50–2.2 (2.28–2.20)	50–2.2 (2.28–2.20)	50–2.2 (2.28–2.20)
I / σ_I	18.3 (6.1)	20.1 (9.6)	19.9 (9.5)	18.2 (8.5)
R_{sym} (%)	5.6 (21.6)	5.3 (14.2)	5.3 (14.5)	5.5 (15.9)
Completeness (%)	98.8 (93.7)	93.9 (92.3)	94.0 (91.8)	93.3 (88.9)
Redundancy	4.5 (4.0)	5.3 (4.8)	5.2 (4.7)	5.2 (4.7)
Refinement				
Resolution (Å)	30–2.0			
No. of reflections	18,432			
R_{work} / R_{free}	22.4 / 24.8			
No. of non-hydrogen atoms / Mean B-factor ($Å^2$)				
Protein	861 / 43.3			
Water	113 / 48.8			
R.m.s. deviations				
Bond lengths (Å)	0.007			
Bond angles (°)	1.26			
Ramachandran plot (%)				
Most favorable	100			
Allowed	0			
Generously allowed	0			
Disallowed	0			

Supplementary references

S1. P. Sheffield, S. Garrard, Z. Derewenda, *Protein Expr. Purif.* **15**, 34-39 (1999).
S2. J. Lebowitz, M. S. Lewis, P. Schuck, *Protein Sci.* **11**, 2067-2079 (2002).
S3. P. Schuck, *Analytical Biochemistry* **320**, 104-124 (2003).
S4. T. C. Terwilliger, J. Berendzen, *Acta Crystallogr. Sect. D-Biol. Crystallogr.* **55**, 849-861 (1999).
S5. T. C. Terwilliger, *Acta Crystallogr. Sect. D-Biol. Crystallogr.* **56**, 965-972 (2000).
S6. P. Emsley, K. Cowtan, *Acta Crystallogr. Sect. D-Biol. Crystallogr.* **60**, 2126-2132 (2004).
S7. A. T. Brunger *et al.*, *Acta Crystallogr. Sect. D-Biol. Crystallogr.* **54**, 905-921 (1998).
S8. W. M. Zhao, A. Seki, G. W. Fang, *Mol. Biol. Cell* **17**, 3881-3896 (2006).
S9. I. Martinez-Garay, A. Rustom, H. H. Gerdes, K. Kutsche, *Genomics* **87**, 243-253 (2006).
S10. M. Fabbro *et al.*, *Dev. Cell* **9**, 477-488 (2005).
S11. A. Lupas, M. Vandyke, J. Stock, *Science* **252**, 1162-1164 (1991).
S12. E. Morita *et al.*, *Embo J.* **26**, 4215-4227 (2007).
S13. W. Blankenfeldt, N. H. Thoma, J. S. Wray, M. Gautel, I. Schlichting, *Proc. Natl. Acad. Sci. U. S. A.* **103**, 17713-17717 (2006).
S14. M. S. Kostelansky *et al.*, *Cell* **129**, 485-498 (2007).
S15. O. Pornillos, S. L. Alam, D. R. Davis, W. I. Sundquist, *Nat Struct Biol* **9**, 812-817 (2002).
S16. R. D. Fisher *et al.*, *Cell* **128**, 841-852 (2007).
S17. J. Mccullough, R. D. Fisher, F. G. Whitby, W. I. Sundquist, C. P. Hill, *Proc Natl Acad Sci U S A* **105**, 7687-7691 (2008).